NANO LETTERS

pubs.acs.org/NanoLett Letter

Ultrasensitive Detection of SARS-CoV-2 Antibody by Graphene Field-Effect Transistors

Hua Kang, Xuejun Wang, Mingquan Guo, Changhao Dai, Renzhong Chen, Lei Yang, Yanling Wu, Tianlei Ying, Zhaoqin Zhu,* Dapeng Wei, Yunqi Liu, and Dacheng Wei*

Cite This: *Nano Lett.* 2021, 21, 7897−7904 Read Online

ACCESS | Metrics & More | Article Recommendations | Supporting Information

ABSTRACT: The fast spread of SARS-CoV-2 has severely threatened the public health. Establishing a sensitive method for SARS-CoV-2 detection is of great significance to contain the worldwide pandemic. Here, we develop a graphene field-effect transistor (g-FET) biosensor and realize ultrasensitive SARS-CoV-2 antibody detection with a limit of detection (LoD) down to 10^{-18} M (equivalent to 10^{-16} g mL^{-1}) level. The g-FETs are modified with spike S1 proteins, and the SARS-CoV-2 antibody biorecognition events occur in the vicinity of the graphene surface, yielding an LoD of ∼150 antibodies in 100 μL full serum, which is the lowest LoD value of antibody detection. The diagnoses time is down to 2 min for detecting clinical serum samples. As such, the g-FETs leverage rapid and precise SARS-CoV-2 screening and also hold great promise in prevention and control of other epidemic outbreaks in the future.

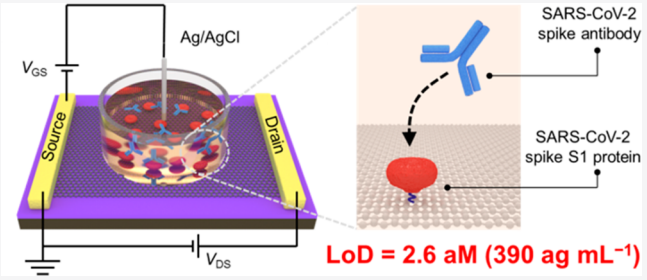

KEYWORDS: *field-effect transistor, biosensor, SARS-CoV-2, spike S1 protein, antibody*

INTRODUCTION

The outspreading of COVID-19 poses a great threat to public health. Precise diagnoses of COVID-19 are crucial in the pandemic control to minimize the far-reaching impact on global society and economy. At present, the golden standard for COVID-19 diagnoses is nucleic acid testing by quantitative reverse transcription-polymerase chain reaction (qRT-PCR).[1−4] However, qRT-PCR requires time-consuming purification and amplification procedures, costly instrumentation, and professional technicians,[5] which significantly lower the testing efficiency. Thus, it is extremely important to develop a rapid and easy-operated method to speed the COVID-19 testing. The detection of SRAS-CoV-2 virus-mediated immune antibody provides another choice to diagnose the infection as well as its current status with simple, fast, and low-cost features.[5,6] In addition, detecting the neutralizing antibody level after vaccination is also necessary to evaluate the effectiveness of SARS-CoV-2 vaccine.[1,7,8]

Until now, antibody detection methods including colloidal gold nanoparticle-based lateral-flow assay,[3] enzyme-linked immunosorbent assay,[6] luminescence-based biosensor,[9] and 3D-printed electrochemical approach[10] have been established. However, limit of detection (LoD) for monitoring antibodies including SARS-CoV-2 antibodies rarely reaches 2.8 fM (1 fM = 10^{-15} M),[10] leading to a risk of misdiagnosis when the SARS-CoV-2 antibody concentration is below this value. From the perspective of vaccine efficacy assessment, the sensitivity of existing detection methods induces hardness in estimating the exact time of the neutralizing antibody generation after vaccination. Therefore, ultrasensitive antibody detection is highly demanded for not only COVID-19 diagnoses but also vaccine development.

Here, we develop a graphene field-effect transistor (g-FET) biosensor for ultrasensitive SARS-CoV-2 antibody detection. After immobilizing SARS-CoV-2 spike S1 proteins on the graphene surface as the probes, the g-FET efficiently converts the specific binding of SARS-CoV-2 antibodies into the conductance changes in the graphene channel. Thus, the g-FET detects SARS-CoV-2 antibody with an ultralow LoD down to 2.6 aM (1 aM = 10^{-18} M), equivalent to 390 ag mL^{-1} (1 ag = 10^{-18} g). As an application, the g-FETs are used to detect serum samples from qRT-PCR confirmed COVID-19 patients within a diagnoses time as short as 2 min.

RESULTS AND DISCUSSION

The biosensor is a liquid-gated FET with an Ag/AgCl reference electrode inserted in the electrolyte as the gate electrode (Figure 1a,b). The drain-source current (I_{DS}) flowing through the channel can be controlled by the liquid-gate bias

Received: February 27, 2021
Revised: September 24, 2021
Published: September 28, 2021

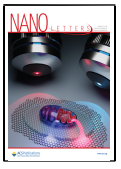

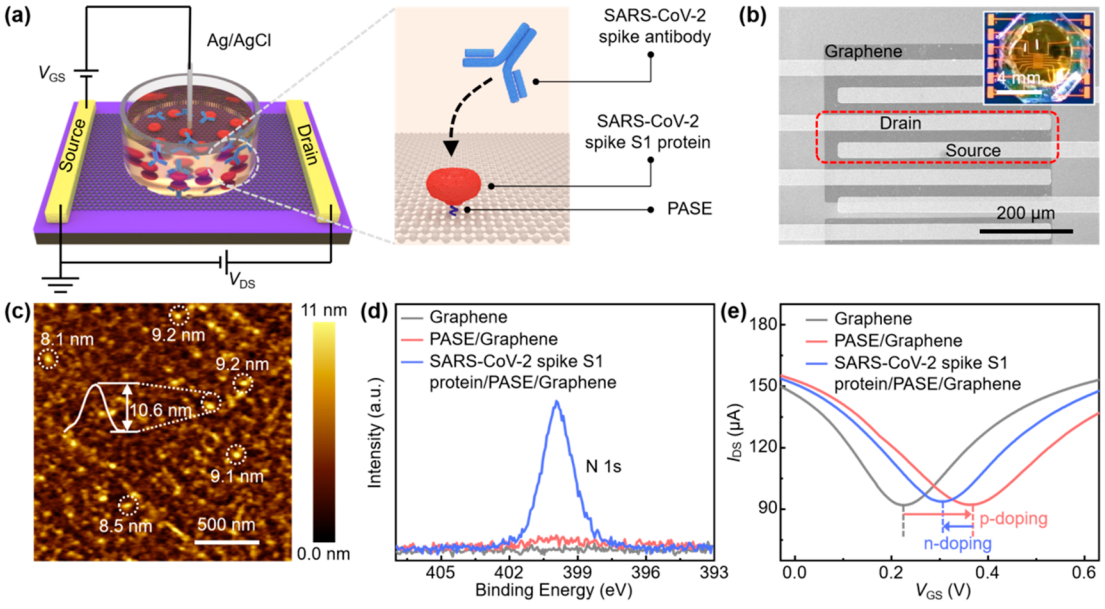

Figure 1. G-FET biosensor for SARS-CoV-2 spike antibody detection. (a) Schematic diagram of the g-FET biosensor. (b) SEM image of the sensing region. The inset is a photograph of a packaged g-FET device with a PDMS well. (c) AFM image of graphene uniformly modified with SARS-CoV-2 spike S1 proteins. (d) XPS N 1s peak of graphene after each functionalization step. (e) Transfer characteristic curves of a g-FET at each immobilization step.

(V_{GS}), where the electrical double layer forms at the electrolyte/graphene interface serving as the dielectric layer. The graphene channel is biochemically functionalized for SARS-CoV-2 antibody recognition. 1-Pyrenebutyric acid *N*-hydroxysuccinimide ester (PASE) molecules are noncovalently coupled to graphene through $\pi-\pi$ interactions as the linkers,[11] and subsequently the spike S1 proteins are anchored on the graphene surface via the reaction between the amine groups on protein and hydroxyl-free succinimide esters on PASE. X-ray photoelectron spectroscopy (XPS) of graphene displays appreciable N 1s peak after modifying PASE molecules rather than pristine graphene, and the N 1s peak is enhanced when proteins are immobilized in Figure 1d (the blue region in Figure S3). In addition, the surface immobilization is studied by measuring the transfer characteristic curve ($I_{DS}-V_{GS}$) of the g-FET at each step (Figure 1e). Dirac point (V_{Dirac}), the V_{GS} value when I_{DS} reaches its minimum, shifts from 226 to 362 and 306 mV after being modified with PASE and proteins, respectively. Meanwhile, atomic force microscope (AFM) image shows that the graphene surface is entirely covered by spike S1 proteins with an average height of 9.1 nm (Figure 1c), which is consistent with previous literatures.[12,13] All of these characterizations reveal successful surface immobilization of graphene with spike S1 proteins.

SARS-CoV-2 genomes encode four main proteins including spike, nucleo, membrane, and envelope proteins.[14,15] In particular, spike antigen protein has been proven to feature higher sensitivity in terms of antibody detection due to its earlier immune response than that of other proteins.[15,16] When integrated with g-FETs, the strong specific binding between antibodies and spike S1 proteins contributes to the sensitive detection of SARS-CoV-2 antibody.[17] Meanwhile, the SARS-CoV-2 spike antibody with an isoelectric point of 6.47 is negatively charged in fetal bovine serum (FBS) with a pH value of 6.8−7.8 (Figure 2a), whereas spike S1 protein is positively charged with an isoelectric point of 8.28. Thus, there is a strong electrostatic attraction force between spike S1 protein and the antibody. With atomic thickness and high surface-to-volume ratio, the g-FET biosensor possesses a high receptor load, and all of the charge carriers flow merely on the graphene surface and are exposed directly to the external environment, ensuring a much higher sensitive response to specific perturbations compared with bulk materials.[18−20] Importantly, turbulent diffusion induced by the sample addition benefits faster antibody diffusion, enabling detection of a low-concentration antibody within several minutes (Supporting Information (SI) Note 4 and Figures S6 and S7). Moreover, drain-source voltage generates local electric field within the Debye length, which might attract negatively charged antibodies for effective biorecognition at the sensing interface. The above factors contribute to the ultrasensitive SARS-CoV-2 antibody detection. Once the antibody is specifically recognized on the graphene surface, it serves as the electron donor to the graphene channel and shifts the Fermi level to the hole conduction band (the inset of Figure 2c), resulting in an n-type doping to graphene. Thus, antigen−antibody binding induces a change of carrier concentration in the graphene channel, yielding a measurable electrical response.

To demonstrate the sensing capability of g-FETs, the device is exposed to SARS-CoV-2 spike antibody in 100 μL FBS with increasing concentrations from 5 aM to 5 pM (1 pM = 10^{-12} M). Surprisingly, the SARS-CoV-2 spike S1 protein modified g-FETs feature appreciable antifouling capability. Before and after 15 min FBS incubation, Dirac point of bare g-FETs shifts by 22 mV, while $|\Delta V_{Dirac}|$ ($\Delta V_{Dirac} = V_{Dirac} - V_{Dirac,0}$, where $V_{Dirac,0}$ corresponds to the value before sample addition) is neglected in the case of protein modified g-FETs (SI Note 5 and Figure S8), indicating the antifouling nature.[21] After addition of the antibody solution, the device is incubated for 15 min to reach a binding equilibrium state. A consecutive left-shift of V_{Dirac} is observed (Figure 2b), verifying the n-type doping upon antigen−antibody binding. Appreciable $|\Delta V_{Dirac}|$ response around 8 mV is observed upon 5 aM antibody, and

https://doi.org/10.1021/acs.nanolett.1c00837
Nano Lett. 2021, 21, 7897−7904

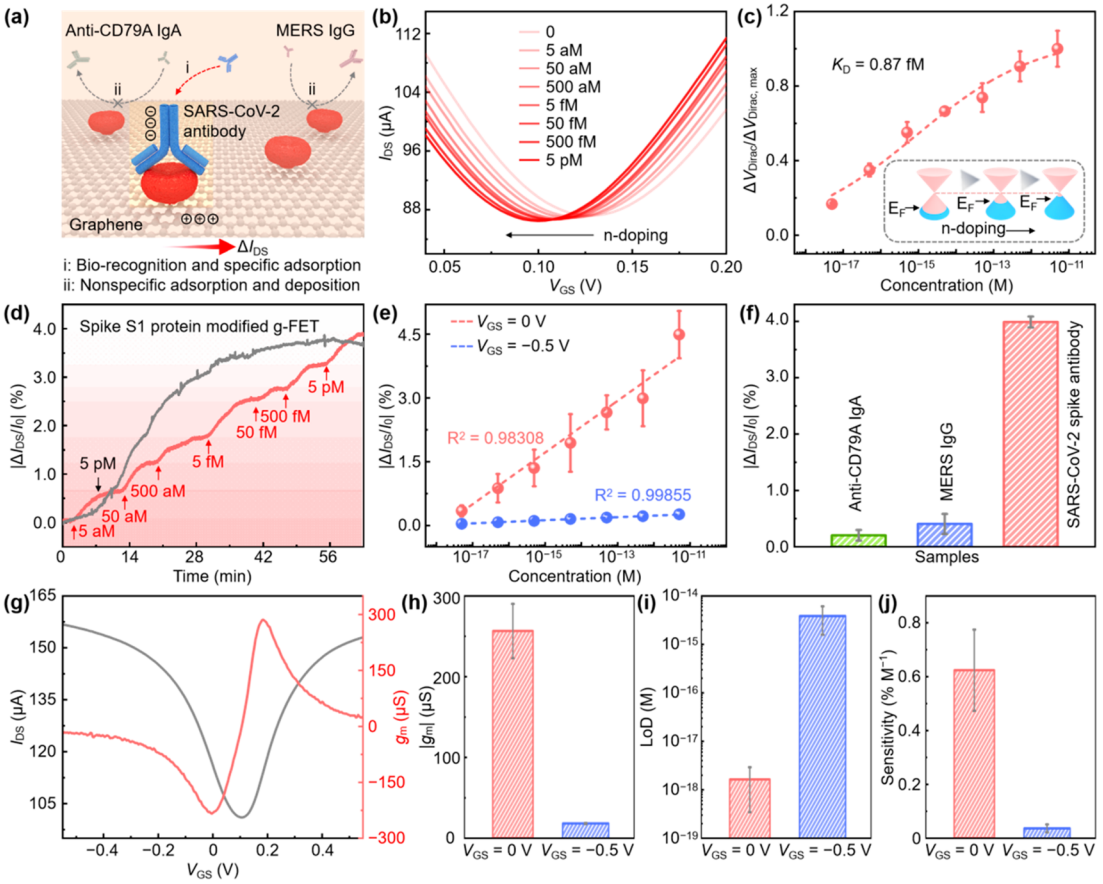

Figure 2. Detection of SARS-CoV-2 spike antibody. (a) Schematic illustration of SARS-CoV-2 spike antibody biorecognition. (b) Transfer characteristics measured after exposing the g-FET biosensor to SARS-CoV-2 spike antibody with increasing concentrations from 5 aM to 5 pM. (c) $\Delta V_{Dirac}/\Delta V_{Dirac,max}$ as a function of antibody concentration. The inset shows the shift of Fermi level as the antibody concentration increases. Error bars represent the standard deviation obtained from three devices. (d) Time-resolved $|\Delta I_{DS}/I_0|$ of spike S1 protein modified g-FET upon SARS-CoV-2 spike antibody by consecutive additions from 5 aM to 5 pM (red line) and direct addition of 5 pM (gray line) to a fresh sensor. (e) $|\Delta I_{DS}/I_0|$ response as a function of antibody concentration in logarithm scale at V_{GS} = 0 V and −0.5 V, respectively. Error bars are obtained from three devices. (f) $|\Delta I_{DS}/I_0|$ response upon anti-CD79A IgA (500 aM), MERS IgG (500 aM) and SARS-CoV-2 spike antibody (50 aM) solutions in FBS. Error bars are obtained from three devices. (g) The dependence of I_{DS} and g_m on V_{GS} at V_{DS} = 0.05 V. Comparison of transconductance (h), LoD (i), and sensitivity (j) at V_{GS} = 0 and −0.5 V, respectively. Error bars are obtained from three devices.

overall 28 mV for the whole concentration range. The equilibrium dissociation constant (K_D) is extracted from the $\Delta V_{Dirac}/\Delta V_{Dirac,\,max}$ versus antibody concentration curve in Figure 2c (here, $\Delta V_{Dirac,\,max} = V_{Dirac,max} - V_{Dirac,0}$ and $V_{Dirac,max}$ is the V_{Dirac} at 5 pM antibody) to evaluate the binding affinity between SARS-CoV-2 spike S1 protein and antibody (SI Note 7 and Figure S10). The relationship between $\Delta V_{Dirac}/\Delta V_{Dirac,\,max}$ and antibody concentration can be described by the Hill-Langmuir model[22]

$$\frac{\Delta V_{Dirac}}{\Delta V_{Dirac,max}} = A\frac{(C_{antibody}/K_D)^n}{1 + (C_{antibody}/K_D)^n} \quad (1)$$

where A is the saturation response coefficient of the protein modified g-FET biosensor, $C_{antibody}$ is the SARS-CoV-2 antibody concentration, and n is the Hill coefficient reflecting the binding cooperativity. In accordance with the fitted curve, K_D is estimated to be 0.87 fM, indicating the strong binding tendency. The reproducibility is above 90% for detecting different concentrations of the SARS-CoV-2 spike antibody (SI Note 6 and Figure S9).

Subsequently, time-resolved $|\Delta I_{DS}/I_0|$ response ($\Delta I_{DS} = I_{DS} - I_0$, where I_0 is the initial I_{DS}) of the g-FET biosensor upon SARS-CoV-2 spike antibody is monitored in FBS at V_{GS} = 0 V (Figure 2d). A $|\Delta I_{DS}/I_0|$ response of 0.6% is observed upon 5 aM antibody, and it increases to 4% when the concentration reaches 5 pM (red curve). A small current drift exists in the measurement, which is probably attributed to the influences from environment temperature, ion concentration, pH value, and so forth.[23] To ensure the accuracy of the measurement, the drift must be controlled within an acceptable range.[24−27] Here, the real-time $|\Delta I_{DS}/I_0|$ response upon addition of 500 aM analytes is 1.72% at approximately the 27th min, and the drift is only 0.06% after 3 min (Figures 2d and S11). Considering the large response, 0.06% drift is neglectable, and the drain source current reaches saturation at approximately the 30th min. All of the drifts are small, which are 0.03%, 0.02%, 0.07%, 0.02%, 0.08% and 0.05% for 5 aM, 50 aM, 5 fM, 50 fM, 500 fM, and 5 pM antibodies, respectively. As a comparison, bare g-FET has no obvious response to SARS-CoV-2 spike antibody from 5 aM to 5 pM (Figure S12), proving that the electrical response comes from specific binding of SARS-CoV-2 spike antibodies rather than nonspecific adsorption on the graphene surface. Three repeated measurements with different devices (Figure 2e) show a linear correlation between $|\Delta I_{DS}/I_0|$ and the antibody concentration in logarithm scale (SI Note 8). It is

https://doi.org/10.1021/acs.nanolett.1c00837
Nano Lett. 2021, 21, 7897−7904

Table 1. Summary of the Existing Antibody Testing Methods

methods	antibody type	LoD or detection limit	response time	specimen	reproducibility	clinical verification	diagnostic sensitivity	ref.
electrochemical enzyme-linked immunosorbent assay	HIV antibody	6.7×10^{-12} M	5 min (6.7×10^{-9} M)	serum		yes	100%	39
lateral flow-based assay	Ebola antibody	~1.3×10^{-9} M	15 min (1.3×10^{-9} M)	serum		yes	100%	40
bead-based immunoassay	Concanavalin A antibody	2.6×10^{-8} M	<60 min (2.6×10^{-8} M)	cell supernatants		no		41
electrochemical DNA-based platform	antidinitrophenol antibody	1.0×10^{-9} M	<10 min (1.0×10^{-7} M)	serum		no		42
black phosphorus-based FET	Human IgG	~6.7×10^{-11} M	seconds (6.7×10^{-11} M)	PBS		no		43
thermally reduced graphene oxide FET	Human IgG	~1.3×10^{-12} M		PBS		no		31
vertically oriented graphene FET	Human IgG	1.3×10^{-11} M	seconds (1.3×10^{-11} M)	PBS		no		44
aptamer-modified graphene FET	IgE	2.9×10^{-10} M	seconds (2.9×10^{-10} M)	PBS		no		25
colloidal gold nanoparticle-based lateral-flow assay	SARS-CoV-2 antibody	qualitative		serum		yes	100%	3
luminescence-based biosensor	SARS-CoV-2 antibody	2.9×10^{-9} M	<5 min (1.3×10^{-8} M)	serum/plasma		yes		9
3D-printed electrochemical test chip	SARS-CoV-2 antibody	2.8×10^{-15} M	12 s (2.8×10^{-15} M)	PBS	>90%	no		10
magnetic immuno-detection assay	SARS-CoV-2 antibody	~2.2×10^{-11} M	42 min (2.2×10^{-11} M)	serum		no		45
enzyme-linked immunosorbent assay	SARS-CoV-2 antibody	~2.7×10^{-11} M	161 min (2.7×10^{-11} M)	serum		no		45
near-infrared-fluorescence amplification method	SARS-CoV-2 antibody	~1.1×10^{-11} M		serum/saliva		yes	100%	1
electrochemical impedance-based detector	SARS-CoV-2 antibody	~6.7×10^{-10} M	seconds (6.7×10^{-10} M)	buffer		yes	100%	46
surface plasmon resonance sensing method	SARS-CoV-2 antibody	6.0×10^{-9} M	15 min (6.0×10^{-9} M)	serum		no		47
paper-based electrochemical biosensor	SARS-CoV-2 antibody	~6.4×10^{-12} M	30 min (6.4×10^{-12} M)	serum	>90%	yes	100%	28
vertical flow cellulose-based assay	SARS-CoV-2 antibody	5.0×10^{-9} M		serum		yes	100%	48
nonradiative energy transfer assay	SARS-CoV-2 antibody	~2.0×10^{-14} M	42 min (2.0×10^{-14} M)	PBS		yes	100%	29
SARS-CoV-2 spike S1 protein modified g-FET	SARS-CoV-2 antibody	2.6×10^{-18} M	<2 min (5.0×10^{-18} ~5.0×10^{-12} M)	serum	>90%	yes	100%	this work

noted that due to the affinity binding $|\Delta I_{DS}/I_0|$ response is up to 3.8% upon direct addition of 5 pM antibody solution (gray curve in Figure 2d), which is similar to the response (4%) upon 5 pM by consecutive additions from 5 aM to 5 pM (Figure S13). The response time decreases from ~2 min (5×10^{-18} M) to ~1 min (5×10^{-12} M) for g-FETs (SI Note 9 and Figure S14). In terms of SARS-CoV-2 antibody detection (Table 1), g-FETs have a response time of ~80 s in serum at 10^{-15} M level, comparable to that of 3D-printed electrochemical test chip[10] in PBS at the same level of concentration. The response time of g-FETs is <2 min upon 5×10^{-18} ~ 5×10^{-12} M antibody, faster than paper-based electrochemical biosensor[28] (30 min for 6.4×10^{-12} M) and nonradiative energy transfer assay[29] (42 min for 2×10^{-14} M). The fast response is attributed to the large association rate (K_{on}), which is calculated by

$$K_{on} = \frac{\Delta I\%_2 - \Delta I\%_1}{t_2 - t_1} \quad (2)$$

where t_1 and t_2 are the time of adding the sample and after a while; $\Delta I\%_1$ and $\Delta I\%_2$ are $|\Delta I_{DS}/I_0|$ values at t_1 and t_2, respectively. According to Figure 2d, K_{on} is estimated to be 0.10908% min^{-1} (5 aM), 0.11742% min^{-1} (50 aM), 0.11202% min^{-1} (500 aM), 0.11274% min^{-1} (5 fM), 0.10002% min^{-1} (50 fM), 0.12% min^{-1} (500 fM) and 0.123% min^{-1} (5 pM). The association (K_{on}) and dissociation (K_{off}) rate constants describe how quickly the antibody associates with and dissociates from the protein, respectively. These values strongly depend on the number and quality of all atomic interactions within the binding pocket as well as K_D of the related antibody−antigen systems.[30] The specificity of SARS-CoV-2 spike S1 protein toward SARS-CoV-2 antibody and its analogues anti-CD79A IgA and middle east respiratory syndrome (MERS) IgG is evaluated. The $|\Delta I_{DS}/I_0|$ of 50 aM SARS-CoV-2 antibody is 4%, while it is smaller than 0.4% for control analytes (anti-CD79A IgA and MERS IgG) at 500 aM, even with 10-fold concentration (Figures 2f and S15). The high $|\Delta I_{DS}/I_0|$ response of 4% at 50 aM might be attributed to the variation of material quality, device fabrication, probe density, as well as high sensitivity of graphene.

LoD is calculated as the concentration generating a $|\Delta I_{DS}/I_0|$ response equal to three times the average noise level (~0.05%). As such, the LoD obtained from the linear standard curve is ~2.6×10^{-18} M (3.9×10^{-16} g mL^{-1}) (Figure S16)

https://doi.org/10.1021/acs.nanolett.1c00837
Nano Lett. 2021, 21, 7897−7904

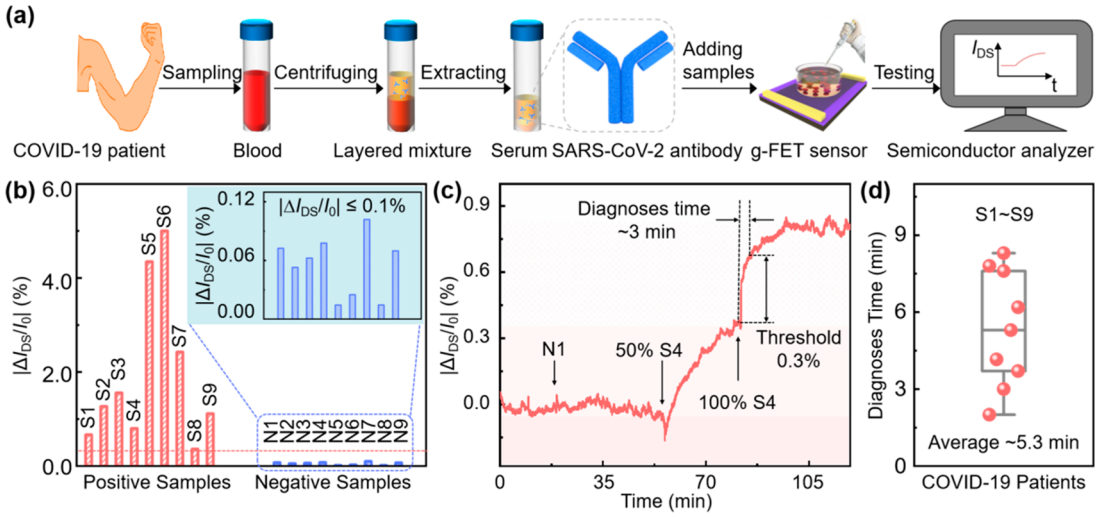

Figure 3. Measurements of clinical samples. (a) Workflow of SARS-CoV-2 antibody detection by spike S1 protein modified g-FET biosensors. (b) $|\Delta I_{DS}/I_0|$ response to clinical samples S1−S9 and N1−N9. The red dashed line denotes the cutoff value of 0.3%. (c) Real-time $|\Delta I_{DS}/I_0|$ signal response upon addition of the clinical samples N1 and S4. (d) Box plot of the diagnoses time for S1−S9.

when $|\Delta I_{DS}/I_0|$ reaches the threshold of ∼0.15%. As a comparison (Table 1), existing technologies hardly reach a LoD of 2.8×10^{-15} M for antibody detection,[10] and the LoD of antibody FET sensors is normally larger than 1.3×10^{-12} M.[31] The spike S1 protein modified g-FET biosensor achieves the lowest LoD value in serum for detecting not only SARS-CoV-2 antibody but also other antibodies up to date. The LoD and the sensitivity depend on the carrier mobility μ, and μ is linearly correlated with the transconductance g_m described as[32]

$$g_m = \frac{W}{L} c\mu V_{DS} \tag{3}$$

where g_m is the steepness of the $I_{DS}-V_{GS}$ curve (Figure 2g), W and L are the channel width and length, c is the gate capacitance. At V_{GS} = 0 V, the average $|g_m|$ estimated from 10 devices is 256 μS with a standard deviation of 33 μS (Figures S17 and 2h), indicating small device-to-device deviation. The LoD and sensitivity obtained by repeatedly measuring different devices have small deviation at V_{GS} = 0 V (Figure 2i,j), indicating appreciable reproducibility. At V_{GS} = −0.5 V, the $|g_m|$ is only 18 μS. The sensitivity and LoD decrease by 1 and 3 orders of magnitude, respectively, compared with V_{GS} = 0 V. As such, the LoD and sensitivity closely depend on the g_m value at a certain V_{GS}.

As an application, we measure clinical serum samples, including S1−S9 collected from venous blood of qRT-PCR confirmed COVID-19 patients, and N1−N9 collected from qRT-PCR negative participants (Figure 3a). One hundred microliters of human serum is served as the buffer in the polydimethylsiloxane (PDMS) reservoir. After totally replacing the buffer by the testing sample, the $|\Delta I_{DS}/I_0|$ response is recorded simultaneously. COVID-19 positive and negative samples are diagnosed by setting the cutoff value at three times of the maximum value of negative samples which is 0.3%. Hence, clinical samples with $|\Delta I_{DS}/I_0| > 0.3\%$ are diagnosed as positive and $|\Delta I_{DS}/I_0| < 0.3\%$ as negative. The g-FETs yield overall $|\Delta I_{DS}/I_0| \geq 0.36\%$ upon S1−S9 and neglectable $|\Delta I_{DS}/I_0| \leq 0.1\%$ upon N1−N9 (Figure 3b). In particular, the $|\Delta I_{DS}/I_0|$ response up to 0.37% is measured when the g-FET is exposed to 50% diluted S4, indicating high sensitivity of the g-FETs in clinical testing (Figure 3c). The diagnostic sensitivity is defined as the true positive rate, which equals to the number of true positives/(the number of true positives + the number of false negatives). The results fully match the qRT-PCR results with a diagnostic sensitivity almost 100%.[33,34] The diagnoses time is estimated by setting the threshold of $|\Delta I_{DS}/I_0|$ response to 0.3%, which is 3-folds of the maximum $|\Delta I_{DS}/I_0|$ to the control samples N1−N9. The average diagnoses time is 5.3 min (Figure 3d) with the shortest only 2 min, indicating the great potential of spike S1 protein modified g-FETs in real-world applications of rapid massive screening of possible SARS-CoV-2 infections.

CONCLUSIONS

In this work, the g-FETs realize ultrasensitive detection of SARS-CoV-2 spike antibody, including clinical samples, with a LoD down to aM-level. Compared with the established technologies, the functionalized g-FETs achieve the highest sensitivity, which could reduce the probability of misdiagnosis in practical applications. The detection result is read out directly from the electrical response without the need of complex operations or data processing. The detection chips can be fabricated by semiconductor manufacturing processes with relatively low cost and integrated into portable systems. Thus, it holds great promise for on-site and point-of-care detection of SARS-CoV-2 and enables one to monitor the infection status in customs, stations, clinics, at home, or even on the Internet, reducing the risk of cross-infection and ensuring the safe world reopening. Moreover, because of the high sensitivity it can be used to estimate the neutralizing antibody level after vaccination in the development of vaccine. Apart from COVID-19, the g-FETs have the feasibility to detect other emerging viral diseases and show great potential for future applications in precision medicine and epidemical control.

EXPERIMENTAL SECTION

Materials and Chemicals. Large area monolayer graphene films were prepared by chemical vapor deposition on copper foils. PASE linkers were obtained from Shanghai Aladdin Biochemical Technology Co., Ltd. SARS-CoV-2 spike S1 protein and SARS-CoV-2 spike antibody were ordered from

https://doi.org/10.1021/acs.nanolett.1c00837
Nano Lett. 2021, 21, 7897−7904

Sino Biological, Inc. Anti-CD79A IgA antibody was purchased from Sangon Biotech (Shanghai) Co., Ltd. MERS IgG antibody was prepared by the previously reported method.[35] The FBS was received from Zhejiang Tianhang Biotechnology Co., Ltd. The serum samples from COVID-19 patients and COVID-19 negative participants were inactivated by heating at 56 °C for 30 min and stored at −20 °C for further detection. The clinical experiments were approved by Shanghai Public Health Clinical Center Ethics Committee (Ethical approval ID: YJ-2020-S080-02).

Characterization. AFM (XE7, Parks System) was employed to measure the surface topography of graphene before and after functionalization. Raman spectrum for bare and PASE-functionalized graphene was measured by HORIBA XploRA with a 532 nm laser. LaB6 scanning electron microscope (SEM) by VEGA 3 XMU was performed to characterize the morphology of channel graphene and drain-source electrodes. The chemical binding component was measured by XPS (Thermo Fisher Scientific K-Alpha instrument) with an Al X-ray source ($h\nu$ = 1486.6 eV).

Fabrication of the g-FET Biosensor. The wetting method was adopted to transfer graphene from copper foil to 300 nm SiO_2/Si substrate on which electrodes (30 μm × 460 μm) were processed with photolithography. Cr/Au (5 nm/38 nm) layers were deposited by thermal evaporation and lift-off techniques. Wire bonding was used to connect the g-FET device with the chip carrier. Phenyl methyl ether solution of poly(methyl methacrylate) (PMMA) was spin-coated on bare graphene on the Cu foil at 3000 rpm for 40 s followed by baking at 180 °C for 1 min. By electrochemical bubbling method,[36,37] graphene was peeled off from Cu foil at 2.3 V using NaOH solution (0.5 M) as the electrolyte. After being rinsed repeatedly with deionized (DI) water, the PMMA/graphene film was transferred onto the SiO_2/Si substrate and dried at room temperature for 1 h following by 180 °C baking for another 2 h. The PMMA carrier layer was dissolved by soaking the device in acetone overnight. The device was washed with ethanol and DI water and dried with N_2 gas. To ensure device consistency, the graphene sheet was patterned into regular rectangle shapes with photolithography and oxygen plasma etching techniques.[38] The g-FET device was immersed in dimethyl sulfoxide solution of PASE at 5 mM for 2 h and sequentially rinsed by ethanol and DI water several times to remove extra residues. Subsequently, the functionalized g-FET device was soaked in phosphate buffer saline (PBS) of 200 nM (1 nM = 10^{-9} M) SARS-CoV-2 spike S1 protein for 6 h. In the end, a PDMS open well with a height of ∼6 mm and height/width ratio (H/W) of 1 was placed on top of the g-FET biosensor device to hold sample solutions.

Device Measurement. Electrical performance measurement was carried out by the semiconductor parameter analyzer (Keysight, B1500A). The antibody samples of different concentrations were prepared by serially diluting the stock solution of SARS-CoV-2 spike antibody. In time-resolved measurement, in order to avoid possible disturbance induced by sample replenishment and ensure efficient turbulent diffusion of antibodies we took out 10 μL solution from the PDMS well and injected 10 μL analyte solution to keep the total volume as 100 μL. We assumed that the current entered saturation until there was no significant change of $|\Delta I_{DS}/I_0|$ above 0.1% for ∼3 min, and then added a new sample with higher concentration. To decrease the drift, we made sure that the measurements were under the same parameters in stable environment. The $I_{DS}-V_{GS}$ curve for SARS-CoV-2 spike antibody was measured by sweeping V_{GS} from 0.04 to 0.20 V at a fixed V_{DS} = 0.05 V. Before testing, the g-FET was immersed in 100 μL FBS for 20 min. Ten microliters of solution was taken out from the PDMS well, and then 10 μL of the antibody solution with higher concentration was injected. After 15 min, the $I_{DS}-V_{GS}$ curve was measured to obtain V_{Dirac}. The time-resolved $|\Delta I_{DS}/I_0|$ response for clinical samples was measured with V_{DS} = 0.05 V and V_{GS} = 0 V. Prior to the clinic testing, the g-FET was soaked in a COVID-19 negative serum sample for 20 min to stabilize the device.

■ ASSOCIATED CONTENT

Supporting Information

The Supporting Information is available free of charge at https://pubs.acs.org/doi/10.1021/acs.nanolett.1c00837.

Detailed information on Raman characterization, XPS characterization, output characteristic characterization, antibody diffusion for ultrasensitive detection, non-specific adsorption characterization, calculation of reproducibility, binding affinity, dependence of signal response on analyte concentration, and calculation of response time (PDF)

■ AUTHOR INFORMATION

Corresponding Authors

Dacheng Wei − *State Key Laboratory of Molecular Engineering of Polymers, Department of Macromolecular Science, Fudan University, Shanghai 200433, China; Institute of Molecular Materials and Devices, Department of Material Science, Fudan University, Shanghai 200433, China; Chongqing School, University of Chinese Academy of Sciences, Chongqing 400714, China;* orcid.org/0000-0003-3593-9897; Email: weidc@fudan.edu.cn

Zhaoqin Zhu − *Department of Laboratory Medicine, Shanghai Public Health Clinical Center, Fudan University, Shanghai 201508, China*; Email: zhaoqinzhu@163.com

Authors

Hua Kang − *State Key Laboratory of Molecular Engineering of Polymers, Department of Macromolecular Science, Fudan University, Shanghai 200433, China; Institute of Molecular Materials and Devices, Department of Material Science, Fudan University, Shanghai 200433, China*

Xuejun Wang − *State Key Laboratory of Molecular Engineering of Polymers, Department of Macromolecular Science, Fudan University, Shanghai 200433, China; Institute of Molecular Materials and Devices, Department of Material Science, Fudan University, Shanghai 200433, China;* orcid.org/0000-0002-7034-0460

Mingquan Guo − *Department of Laboratory Medicine, Shanghai Public Health Clinical Center, Fudan University, Shanghai 201508, China*

Changhao Dai − *State Key Laboratory of Molecular Engineering of Polymers, Department of Macromolecular Science, Fudan University, Shanghai 200433, China; Institute of Molecular Materials and Devices, Department of Material Science, Fudan University, Shanghai 200433, China*

Renzhong Chen − *State Key Laboratory of Molecular Engineering of Polymers, Department of Macromolecular Science, Fudan University, Shanghai 200433, China;*

https://doi.org/10.1021/acs.nanolett.1c00837
Nano Lett. 2021, 21, 7897−7904

Institute of Molecular Materials and Devices, Department of Material Science, Fudan University, Shanghai 200433, China

Lei Yang − *State Key Laboratory of Molecular Engineering of Polymers, Department of Macromolecular Science, Fudan University, Shanghai 200433, China; Institute of Molecular Materials and Devices, Department of Material Science, Fudan University, Shanghai 200433, China*

Yanling Wu − *MOE/NHC/CAMS Key Laboratory of Medical Molecular Virology, School of Basic Medical Sciences, Fudan University, Shanghai 200032, China*

Tianlei Ying − *MOE/NHC/CAMS Key Laboratory of Medical Molecular Virology, School of Basic Medical Sciences, Fudan University, Shanghai 200032, China*

Dapeng Wei − *Chongqing School, University of Chinese Academy of Sciences, Chongqing 400714, China;* orcid.org/0000-0002-3575-617X

Yunqi Liu − *Institute of Molecular Materials and Devices, Department of Material Science, Fudan University, Shanghai 200433, China; Institute of Chemistry, Chinese Academy of Sciences, Beijing 100190, China;* orcid.org/0000-0001-5521-2316

Complete contact information is available at: https://pubs.acs.org/10.1021/acs.nanolett.1c00837

Author Contributions

D.C.W. obtained ideas, supervised the project, and provided the foundation support. H.K. performed the research, analyzed the data. X.W. designed the study, provided guidance in the experimental section, and revised the paper. C.D. assisted in data analysis. R.C. provided help for the figures. L.Y. participated in the format modification. Y.W. and T.Y. supplied the MERS IgG antibody. M.G. and Z.Z. prepared the clinical serum samples. D.P.W. and Y.L. supported the research and commented the manuscript. H.K., X.W., and D.C.W. wrote the manuscript. All authors have given approval to the final version of the manuscript.

Notes

The authors declare no competing financial interest.

■ ACKNOWLEDGMENTS

This work was supported by National Key R&D Program of China (2021YFE0201400), the National Natural Science Foundation of China (51773041 and 61890940), the Strategic Priority Research Program of the Chinese Academy of Sciences (XDB30000000), China Postdoctoral Science Foundation (2019M661353), National Postdoctoral Program for Innovative Talents (BX20190072), Chongqing Talents Program (CQYC2020030146), Chongqing Bayu Scholar Program (DP2020036), and Fudan University.

■ REFERENCES

(1) Liu, T.; Hsiung, J.; Zhao, S.; Kost, J.; Sreedhar, D.; Hanson, C. V.; Olson, K.; Keare, D.; Chang, S. T.; Bliden, K. P.; Gurbel, P. A.; Tantry, U. S.; Roche, J.; Press, C.; Boggs, J.; Rodriguez-Soto, J. P.; Montoya, J. G.; Tang, M.; Dai, H. Quantification of antibody avidities and accurate detection of SARS-CoV-2 antibodies in serum and saliva on plasmonic substrates. *Nat. Biomed. Eng.* **2020**, *4*, 1188−1196.

(2) Moitra, P.; Alafeef, M.; Dighe, K.; Frieman, M. B.; Pan, D. Selective naked-eye detection of SARS-CoV-2 mediated by N gene targeted antisense oligonucleotide capped plasmonic nanoparticles. *ACS Nano* **2020**, *14* (6), 7617−7627.

(3) Huang, C.; Wen, T.; Shi, F.-J.; Zeng, X.-Y.; Jiao, Y.-J. Rapid detection of IgM antibodies against the SARS-CoV-2 virus via colloidal gold nanoparticle-based lateral-flow assay. *ACS Omega* **2020**, *5* (21), 12550−12556.

(4) Hosseini, A.; Pandey, R.; Osman, E.; Victorious, A.; Li, F.; Didar, T.; Soleymani, L. Roadmap to the bioanalytical testing of COVID-19: from sample collection to disease surveillance. *ACS Sens.* **2020**, *5* (11), 3328−3345.

(5) Li, Z.; Yi, Y.; Luo, X.; Xiong, N.; Liu, Y.; Li, S.; Sun, R.; Wang, Y.; Hu, B.; Chen, W.; Zhang, Y.; Wang, J.; Huang, B.; Lin, Y.; Yang, J.; Cai, W.; Wang, X.; Cheng, J.; Chen, Z.; Sun, K.; Pan, W.; Zhan, Z.; Chen, L.; Ye, F. Development and clinical application of a rapid IgM-IgG combined antibody test for SARS-CoV-2 infection diagnosis. *J. Med. Virol.* **2020**, *92*, 1518−1524.

(6) Carter, L. J.; Garner, L. V.; Smoot, J. W.; Li, Y.; Zhou, Q.; Saveson, C. J.; Sasso, J. M.; Gregg, A. C.; Soares, D. J.; Beskid, T. R.; Jervey, S. R.; Liu, C. Assay techniques and test development for COVID-19 diagnosis. *ACS Cent. Sci.* **2020**, *6* (5), 591−605.

(7) Muruato, A. E.; Fontes-Garfias, C. R.; Ren, P.; Garcia-Blanco, M. A.; Menachery, V. D.; Xie, X.; Shi, P.-Y. A high-throughput neutralizing antibody assay for COVID-19 diagnosis and vaccine evaluation. *Nat. Commun.* **2020**, *11*, 4059.

(8) Koff, W. C.; Schenkelberg, T.; Williams, T.; Baric, R. S.; McDermott, A.; Cameron, C. M.; Cameron, M. J.; Friemann, M. B.; Neumann, G.; Kawaoka, Y.; Kelvin, A. A.; Ross, T. M.; Schultz-Cherry, S.; Mastro, T. D.; Priddy, F. H.; Moore, K. A.; Ostrowsky, J. T.; Osterholm, M. T.; Goudsmit, J. Development and deployment of COVID-19 vaccines for those most vulnerable. *Sci. Transl. Med.* **2021**, *13* (579), No. eabd1525.

(9) Quijano-Rubio, A.; Yeh, H.-W.; Park, J.; Lee, H.; Langan, R. A.; Boyken, S. E.; Lajoie, M. J.; Cao, L.; Chow, C. M.; Miranda, M. C.; Wi, J.; Hong, H. J.; Stewart, L.; Oh, B.-H.; Baker, D. De novo design of modular and tunable protein biosensors. *Nature* **2021**, *591*, 482−487.

(10) Ali, M. A.; Hu, C.; Jahan, S.; Yuan, B.; Saleh, M. S.; Ju, E.; Gao, S.-J.; Panat, R. Sensing of COVID-19 antibodies in seconds via aerosol jet nanoprinted reduced-graphene-oxide-coated 3D electrodes. *Adv. Mater.* **2021**, *33*, 2006647.

(11) Hao, Z.; Wang, Z.; Li, Y.; Zhu, Y.; Wang, X.; De Moraes, C. G.; Pan, Y.; Zhao, X.; Lin, Q. Measurement of cytokine biomarkers using an aptamer-based affinity graphene nanosensor on a flexible substrate toward wearable applications. *Nanoscale* **2018**, *10*, 21681−21688.

(12) Liu, C.; Mendonça, L.; Yang, Y.; Gao, Y.; Shen, C.; Liu, J.; Ni, T.; Ju, B.; Liu, C.; Tang, X.; Wei, J.; Ma, X.; Zhu, Y.; Liu, W.; Xu, S.; Liu, Y.; Yuan, J.; Wu, J.; Liu, Z.; Zhang, Z.; Liu, L.; Wang, P.; Zhang, P. The architecture of inactivated SARS-CoV-2 with postfusion spikes revealed by cryo-EM and cryo-ET. *Structure* **2020**, *28* (11), 1218−1224.

(13) Shang, J.; Wan, Y.; Luo, C.; Ye, G.; Geng, Q.; Auerbach, A.; Li, F. Cell entry mechanisms of SARS-CoV-2. *Proc. Natl. Acad. Sci. U. S. A.* **2020**, *117* (21), 11727−11734.

(14) Parihar, A.; Ranjan, P.; Sanghi, S. K.; Srivastava, A. K.; Khan, R. Point-of-care biosensor-based diagnosis of COVID-19 holds promise to combat current and future pandemics. *ACS Appl. Bio Mater.* **2020**, *3* (11), 7326−7343.

(15) Liu, W.; Liu, L.; Kou, G.; Zheng, Y.; Ding, Y.; Ni, W.; Wang, Q.; Tan, L.; Wu, W.; Tang, S.; Xiong, Z.; Zheng, S. Evaluation of nucleocapsid and spike protein-based enzyme-linked immunosorbent assays for detecting antibodies against SARS-CoV-2. *J. Clin. Microbiol.* **2020**, *58* (6), No. e00461.

(16) Kontou, P. I.; Braliou, G. G.; Dimou, N. L.; Nikolopoulos, G.; Bagos, P. G. Antibody tests in detecting SARS-CoV-2 infection: a meta-analysis. *Diagnostics* **2020**, *10* (5), 319.

(17) Seo, G.; Lee, G.; Kim, M. J.; Baek, S.-H.; Choi, M.; Ku, K. B.; Lee, C.-S.; Jun, S.; Park, D.; Kim, H. G.; Kim, S.-J.; Lee, J.-O.; Kim, B. T.; Park, E. C.; Kim, S. I. Rapid detection of COVID-19 causative virus (SARS-CoV-2) in human nasopharyngeal swab specimens using field-effect transistor-based biosensor. *ACS Nano* **2020**, *14* (4), 5135−5142.

(18) Wang, Z.; Yi, K.; Lin, Q.; Yang, L.; Chen, X.; Chen, H.; Liu, Y.; Wei, D. Free radical sensors based on inner-cutting graphene field-effect transistors. *Nat. Commun.* **2019**, *10*, 1544.
(19) Jiang, Z.; Feng, B.; Xu, J.; Qing, T.; Zhang, P.; Qing, Z. Graphene biosensors for bacterial and viral pathogens. *Biosens. Bioelectron.* **2020**, *166* (15), 112471.
(20) Vu, C.-A.; Chen, W.-Y. Field-effect transistor biosensors for biomedical applications: recent advances and future prospects. *Sensors* **2019**, *19* (19), 4214.
(21) Wang, X.; Zhu, Y.; Olsen, T. R.; Sun, N.; Zhang, W.; Pei, R.; Lin, Q. A graphene aptasensor for biomarker detection in human serum. *Electrochim. Acta* **2018**, *290*, 356−363.
(22) Wang, Z.; Hao, Z.; Wang, X.; Huang, C.; Lin, Q.; Zhao, X.; Pan, Y. A flexible and regenerative aptameric graphene-nafion biosensor for cytokine storm biomarker monitoring in undiluted biofluids toward wearable applications. *Adv. Funct. Mater.* **2021**, *31*, 2005958.
(23) Ushiba, S.; Okino, T.; Miyakawa, N.; Ono, T.; Shinagawa, A.; Kanai, Y.; Inoue, K.; Takahashi, K.; Kimura, M.; Matsumoto, K. State-space modeling for dynamic response of graphene FET biosensors. *Jpn. J. Appl. Phys.* **2020**, *59*, SGGH04.
(24) Pappa, A. M.; Ohayon, D.; Giovannitti, A.; Maria, I. P.; Savva, A.; Uguz, I.; Rivnay, J.; McCulloch, I.; Owens, R. M.; Inal, S. Direct metabolite detection with an n-type accumulation mode organic electrochemical transistor. *Sci. Adv.* **2018**, *4*, No. eaat0911.
(25) Ohno, Y.; Maehashi, K.; Matsumoto, K. Label-free biosensors based on aptamer-modified graphene field-effect transistors. *J. Am. Chem. Soc.* **2010**, *132* (51), 18012−18013.
(26) Myung, S.; Solanki, A.; Kim, C.; Park, J.; Kim, K. S.; Lee, K.-B. Graphene-encapsulated nanoparticle-based biosensor for the selective detection of cancer biomarkers. *Adv. Mater.* **2011**, *23*, 2221−2225.
(27) Byon, H. R.; Choi, H. C. Network single-walled carbon nanotube-field effect transistors (SWNT-FETs) with increased schottky contact area for highly sensitive biosensor applications. *J. Am. Chem. Soc.* **2006**, *128* (7), 2188−2189.
(28) Yakoh, A.; Pimpitak, U.; Rengpipat, S.; Hirankarn, N.; Chailapakul, O.; Chaiyo, S. Paper-based electrochemical biosensor for diagnosing COVID-19: detection of SARS-CoV-2 antibodies and antigen. *Biosens. Bioelectron.* **2021**, *176*, 112912.
(29) Avila-Huerta, M. D.; Ortiz-Riaño, E. J.; Mancera-Zapata, D. L.; Cortés-Sarabia, K.; Morales-Narváez, E. Facile determination of COVID-19 seroconversion via nonradiative energy transfer. *ACS Sens.* **2021**, *6* (6), 2136−2140.
(30) Schwesinger, F.; Ros, R.; Strunz, T.; Anselmetti, D.; Güntherodt, H.-J.; Honegger, A.; Jermutus, L.; Tiefenauer, L.; Plückthun, A. Unbinding forces of single antibody-antigen complexes correlate with their thermal dissociation rates. *Proc. Natl. Acad. Sci. U. S. A.* **2000**, *97* (18), 9972−9977.
(31) Mao, S.; Yu, K.; Lu, G.; Chen, J. Highly sensitive protein sensor based on thermally-reduced graphene oxide field-effect transistor. *Nano Res.* **2011**, *4* (10), 921.
(32) Xu, H.; Zhang, Z.; Xu, H.; Wang, Z.; Wang, S.; Peng, L.-M. Top-gated graphene field-effect transistors with high normalized transconductance and designable Dirac point voltage. *ACS Nano* **2011**, *5* (6), 5031−5037.
(33) Korevaar, D. A.; Gopalakrishna, G.; Cohen, J. F.; Bossuyt, P. M. Targeted test evaluation: a framework for designing diagnostic accuracy studies with clear study hypotheses. *Diagn. Progn. Res.* **2019**, *3*, 22.
(34) Doenhoff, M. J.; Chiodini, P. L.; Hamilton, J. V. Specific and sensitive diagnosis of schistosome infection: can it be done with antibodies? *Trends Parasitol.* **2004**, *20* (1), 35−39.
(35) Ying, T.; Prabakaran, P.; Du, L.; Shi, W.; Feng, Y.; Wang, Y.; Wang, L.; Li, W.; Jiang, S.; Dimitrov, D. S.; Zhou, T. Junctional and allele-specific residues are critical for MERS-CoV neutralization by an exceptionally potent germline-like antibody. *Nat. Commun.* **2015**, *6*, 8223.
(36) Sun, J.; Deng, S.; Guo, W.; Zhan, Z.; Deng, J.; Xu, C.; Fan, X.; Xu, K.; Guo, W.; Huang, Y.; Liu, X. Electrochemical bubbling transfer of graphene using a polymer support with encapsulated air gap as permeation stopping layer. *J. Nanomater.* **2016**, *2016*, 1.
(37) Wang, Y.; Zheng, Y.; Xu, X.; Dubuisson, E.; Bao, Q.; Lu, J.; Loh, K. P. Electrochemical delamination of CVD-grown graphene film: toward the recyclable use of copper catalyst. *ACS Nano* **2011**, *5* (12), 9927−9933.
(38) Hao, Z.; Zhu, Y.; Wang, X.; Rotti, P. G.; DiMarco, C.; Tyler, S. R.; Zhao, X.; Engelhardt, J. F.; Hone, J.; Lin, Q. Real-time monitoring of insulin using a graphene field-effect transistor aptameric nanosensor. *ACS Appl. Mater. Interfaces* **2017**, *9* (33), 27504−27511.
(39) Bhimji, A.; Zaragoza, A. A.; Live, L. S.; Kelley, S. O. Electrochemical enzyme-linked immunosorbent assay featuring proximal reagent generation: detection of human immunodeficiency virus antibodies in clinical samples. *Anal. Chem.* **2013**, *85* (14), 6813−6819.
(40) Brangel, P.; Sobarzo, A.; Parolo, C.; Miller, B. S.; Howes, P. D.; Gelkop, S.; Lutwama, J. J.; Dye, J. M.; McKendry, R. A.; Lobel, L.; Stevens, M. M. A serological point-of-care test for the detection of IgG antibodies against Ebola virus in human survivors. *ACS Nano* **2018**, *12* (1), 63−73.
(41) Ramirez, K.; Campbell, E.; Han, S.-Y.; Buehler, J.; Phan, T.; Young Yoon, H.; Lee, Y. L.; Suresh, T.; Sulchek, T. Optimization of microparticle reagents to collect and detect antibody. *Langmuir* **2019**, *35* (36), 11717−11724.
(42) Rossetti, M.; Brannetti, S.; Mocenigo, M.; Marini, B.; Ippodrino, R.; Porchetta, A. Harnessing effective molarity to design an electrochemical DNA-based platform for clinically relevant antibody detection. *Angew. Chem., Int. Ed.* **2020**, *59*, 14973−14978.
(43) Chen, Y.; Ren, R.; Pu, H.; Chang, J.; Mao, S.; Chen, J. Field-effect transistor biosensors with two-dimensional black phosphorus nanosheets. *Biosens. Bioelectron.* **2017**, *89*, 505−510.
(44) Mao, S.; Yu, K.; Chang, J.; Steeber, D. A.; Ocola, L. E.; Chen, J. Direct growth of vertically-oriented graphene for field-effect transistor biosensor. *Sci. Rep.* **2013**, *3*, 1696.
(45) Pietschmann, J.; Vöpel, N.; Spiegel, H.; Krause, H.-J.; Schröper, F. Brief communication: magnetic immuno-detection of SARS-CoV-2 specific antibodies. *BioRxiv* 2020.06.02, 131102. DOI: 10.1101/2020.06.02.131102(accessed October 15, 2020).
(46) Rashed, M. Z.; Kopechek, J. A.; Priddy, M. C.; Hamorsky, K. T.; Palmer, K. E.; Mittal, N.; Valdez, J.; Flynn, J.; Williams, S. J. Rapid detection of SARS-CoV-2 antibodies using electrochemical impedance-based detector. *Biosens. Bioelectron.* **2021**, *171*, 112709.
(47) Djaileb, A.; Charron, B.; Jodaylami, M. H.; Thibault, V.; Coutu, J.; Stevenson, K.; Forest, S.; Live, L. S.; Boudreau, D.; Pelletier, J. N.; Masson, J.-F. A rapid and quantitative serum test for SARS-CoV-2 antibodies with portable surface plasmon resonance sensing. *ChemRxiv* **2020**, 12118914. https://chemrxiv.org/engage/chemrxiv/article-details/60c749dcbb8c1a400b3daedf (accessed November 07, 2020).
(48) Kim, S.; Hao, Y.; Miller, E. A.; Tay, D. M. Y.; Yee, E.; Kongsuphol, P.; Jia, H.; McBee, M.; Preiser, P. R.; Sikes, H. D. Vertical flow cellulose-based assays for SARS-CoV-2 antibody detection in human serum. *ACS Sens.* **2021**, *6* (5), 1891−1898.

https://doi.org/10.1021/acs.nanolett.1c00837
Nano Lett. 2021, 21, 7897−7904